Vertebrate cells genetically deficient for Cdc14A or Cdc14B retain DNA damage checkpoint proficiency but are impaired in DNA repair

Annamaria Mocciaro,[1] Eli Berdougo,[2] Kang Zeng,[3] Elizabeth Black,[4] Paola Vagnarelli,[5] William Earnshaw,[5] David Gillespie,[4] Prasad Jallepalli,[2] and Elmar Schiebel[1]

[1]Zentrum für Molekulare Biologie der Universität Heidelberg, DKFZ-ZMBH Allianz, 69117 Heidelberg, Germany
[2]Memorial Sloan-Kettering Cancer Center, New York, NY 10065
[3]Cancer Research Centre, University of Liverpool, Liverpool L69 3BX, England, UK
[4]Beatson Institute for Cancer Research, Glasgow G61 1BD, Scotland, UK
[5]Wellcome Trust Centre for Cell Biology, Institute of Cell Biology, University of Edinburgh, Edinburgh EH8 9YL, Scotland, UK

A recent study suggested that human Cdc14B phosphatase has a central function in the G2 DNA damage checkpoint. In this study, we show that chicken DT40, human HCT116, and human telomerase reverse transcription–immortalized retinal pigment epithelial cells deleted for the Cdc14A or Cdc14B gene are DNA damage checkpoint proficient and arrest efficiently in G2 in response to irradiation. Cdc14A knockout (KO) or Cdc14B-KO cells also maintain normal levels of Chk1 and Chk2 activation after irradiation. Surprisingly, however, irradiation-induced γ-H2A.X foci and DNA double-strand breaks persist longer in Cdc14A-KO or Cdc14B-KO cells than controls, suggesting that Cdc14 phosphatases are required for efficient DNA repair.

Introduction

In *Saccharomyces cerevisiae*, the conserved phosphatase Cdc14 regulates late mitotic events (Stegmeier and Amon, 2004) by antagonizing Cdk function to allow exit from mitosis. At anaphase onset, Cdc14 is released from the nucleolus into the nucleoplasm and cytoplasm, and becomes involved in sharpening of the metaphase to anaphase transition, spindle stabilization, chromosomal passenger protein redistribution, segregation of ribosomal DNA, and triggering of mitotic exit (Stegmeier and Amon, 2004; Queralt and Uhlmann, 2008).

Vertebrates possess two isoforms of Cdc14, named Cdc14A and Cdc14B; in hominoids, a gene retro-duplication event gave rise to an additional Cdc14 family member, Cdc14Bretro, whose expression is brain and testis specific (Rosso et al., 2008). Cdc14A localizes at the centrosome in interphase human cells. Its overexpression caused premature centrosome splitting, whereas its depletion induced impaired centrosome separation and failure of cytokinesis (Kaiser et al., 2002; Mailand et al., 2002). Based on RNAi depletion and overexpression experiments, nucleolar human Cdc14B (hCdc14B) has been implicated in mitotic spindle assembly, centriole duplication, and mitotic exit (Kaiser et al., 2002; Mailand et al., 2002; Dryden et al., 2003; Cho et al., 2005; Wu et al., 2008). Recently, Bassermann et al. (2008) suggested that hCdc14B has a central role in the G2 DNA damage checkpoint through regulation of the activity of the anaphase-promoting complex/cyclosome (APC/C) subunit Cdh1.

To obtain a clearer picture of the functions of vertebrate Cdc14 genes, we analyzed avian and human cell lines in which Cdc14A and Cdc14B genes were deleted by gene targeting. We demonstrate that neither Cdc14A nor Cdc14B is essential for a functional G2 DNA damage checkpoint in response to double-strand breaks (DSBs). Instead, cells lacking either phosphatase show elevated levels of spontaneous DNA damage and impaired repair, uncovering a novel role for Cdc14A and Cdc14B.

Correspondence to Prasad Jallepalli: jallepap@mskcc.org; or Elmar Schiebel: e.schiebel@zmbh.uni-heidelberg.de

Abbreviations used in this paper: APC/C, anaphase-promoting complex/cyclosome; cCdc14, chicken Cdc14; DSB, double-strand break; DXR, doxorubicin; hCdc14, human Cdc14; hTERT, human telomerase reverse transcription; IB, immunoblotting; IF, immunofluorescence; IR, γ irradiation; KO, knockout; MI, mitotic index; MTT, method of transcriptional and translational; Noco, nocodazole; PI, propidium iodide; RPE, retinal pigment epithelial; WT, wild type.

The Rockefeller University Press $30.00
J. Cell Biol. Vol. 189 No. 4 631–639
www.jcb.org/cgi/doi/10.1083/jcb.200910057

Results and discussion

Cdc14A- and Cdc14B-deficient DT40 cell lines

Chicken DT40 B-lymphoma cells show high efficiency of targeted integration of transfected constructs, allowing the disruption of genes through homologous recombination (Buerstedde and Takeda, 1991). Therefore, we analyzed the function of Cdc14A and Cdc14B in this cell line.

Computational (GNOMON) analysis of the chicken genome predicts orthologues of Cdc14A (chicken Cdc14A [cCdc14A]; GenBank accession no. NC_006095.2) and Cdc14B (cCdc14B; NCBI Protein database accession no. XP_425045.2) on chromosomes 8 and Z, respectively. However, only parts of these sequences are similar to human and mouse Cdc14 proteins. Therefore, we isolated cCdc14A and cCdc14B cDNAs by RT-PCR from total RNA of DT40 wild-type (WT) cells (unpublished data). These cDNA sequences predict cCdc14A and cCdc14B proteins conserved with other species throughout their length (GU550056 and GU550055). The chicken genome does not possess a Cdc14Bretro gene (Rosso et al., 2008).

cCdc14A was detected at the centrosome of cells in interphase and late mitosis (Fig. S1 A). This localization is consistent with that of hCdc14A (Kaiser et al., 2002; Mailand et al., 2002). We were unable to raise antibodies against cCdc14B protein (unpublished data). Therefore, we generated a DT40 cell line stably expressing cCdc14B-GFP. In agreement with the localization of hCdc14B (Kaiser et al., 2002; Mailand et al., 2002), cCdc14B-GFP localized to the nucleus in interphase cells with an enrichment in the nucleolus (Fig. S1 B). In mitosis, cCdc14B-GFP was dispersed throughout the cell (unpublished data).

Next, we generated cCdc14A knockout (KO) and cCdc14B-KO cell lines (Fig. S1, C–G; and Fig. S2, A–C). Surprisingly, cells lacking either cCdc14A or cCdc14B were viable. Moreover, the doubling time of the cCdc14B-KO cell lines was indistinguishable from that of WT cells (Fig. S2 D). This indicates that cCdc14B is not essential for viability and proliferation of DT40 cells. hCdc14B has been proposed to regulate mitotic exit by interacting with SIRT2 (Dryden et al., 2003). However, the mitotic index (MI) of cCdc14B-KO cells did not show any significant increase indicative of defects in mitotic exit (Fig. S2 E). This is consistent with the lack of a mitotic exit defect of hCdc14B$^{\Delta/\Delta}$ cells (Berdougo et al., 2008).

In cCdc14B-KO cells, the levels of the cCdc14A protein were not increased compared with WT cells, and cCdc14A was still associated with the centrosome (Fig. S2, F and G). Thus, it is unlikely that up-regulation or relocalization of cCdc14A compensate for the loss of cCdc14B.

Avian cells lacking cCdc14A and cCdc14B have a functional DNA damage checkpoint

Recently, it was suggested that hCdc14B is an essential component of the G2 DNA damage checkpoint. In response to genotoxic stress in G2, hCdc14B relocalizes from the nucleolus to the nucleus and activates APC/C^{Cdh1}, leading to degradation of Plk1 and stabilization of claspin. This allows for efficient phosphorylation of the checkpoint kinase Chk1 and checkpoint activation. The role of Cdc14A in the G2 DNA damage checkpoint was not investigated (Bassermann et al., 2008).

In agreement with the data of Bassermann et al. (2008), DT40 cells expressing cCdc14B-GFP after synchronization in G2 and exposure to γ irradiation (IR) showed a relocalization of cCdc14B from the nucleolus to the nucleus (Fig. S3, A and B), whereas cCdc14A remained at the centrosome (Fig. S3, C and D).

Using cCdc14A-KO and cCdc14B-KO DT40 cell lines, we assayed for a defect in the G2 DNA damage checkpoint. As a control for checkpoint deficiency, we used DT40 Chk1-KO cells (Zachos et al., 2003). To quantify G2 checkpoint proficiency, we first added nocodazole (Noco) to the growth medium to trap cells in mitosis. This allowed us to measure the number of cells that entered M phase from G2 by staining for histone 3 phosphorylated on Ser10 (pH3). WT, cCdc14A-KO, cCdc14B-KO, and Chk1-KO DT40 cells were incubated in medium containing Noco for 8 h with or without prior exposure to IR. Chk1-KO cells accumulate in mitosis to a similar extent regardless of prior IR (Zachos et al., 2003). In marked contrast, IR strongly reduced mitotic accumulation in DT40 WT, cCdc14A-KO, and cCdc14B-KO cells, which is indicative of a functional G2 checkpoint (Fig. 1 A, green bars). Similar results were obtained when cells were pulsed for 1 h with the DNA-damaging drug doxorubicin (DXR; unpublished data).

G2 phase–specific activation of APC/C^{Cdh1} after DNA damage was previously reported in DT40 cells (Sudo et al., 2001). To evaluate the importance of Cdh1 for DNA damage–induced cell cycle arrest in G2 in DT40 cells, Cdh1-KO DT40 cells were treated as in Fig. 1 A, and the percentage of mitotic cells (MI) was determined by flow cytometry. Cdh1-KO cells were arrested after IR as efficiently as WT cells (Fig. 1 A, green bars).

The nature of the G2 arrest after DNA damage varies according to the position of a cell in the cell cycle at the time when damage occurs (Xu et al., 2002). Involvement of hCdc14B and APC/C^{Cdh1} in the G2 checkpoint has been suggested specifically for human cells exposed to damage in G2 (Bassermann et al., 2008). To address the possibility that the discrepancies between the phenotype described by Bassermann et al. (2008) after hCdc14B knockdown and our observations in DT40 cCdc14B-KO cells were a result of irradiating populations of asynchronously growing cells, WT, cCdc14A-KO, cCdc14B-KO, Chk1-KO, and Cdh1-KO DT40 cells were synchronized in early S phase with aphidicolin, released for 4 h to allow progression into G2 (Fig. 1 B), and exposed to IR. Under these conditions, cCdc14A-KO, cCdc14B-KO, and Cdh1-KO cells maintained their ability to arrest in G2 after damage as efficiently as WT cells, as shown by the reduction in their MI (Fig. 1 C). To exclude the possibility that the G2 checkpoint proficiency in cCdc14-KO cells was caused by adaptation, we treated transgenic cCdc14A-KO/cCdc14A-HA and cCdc14B-KO/cCdc14B-HA cells with 4-hydroxytamoxifen to activate Cre recombinase and remove the cDNAs encoding cCdc14A-HA or cCdc14B-HA (Fig. S3 E). When G2 checkpoint proficiency was assessed immediately after transgene removal, cells arrested efficiently after IR (Fig. S3 F).

Prolonged G2 arrest after DNA damage induces centrosome amplification in human and DT40 cells, and this amplification is dependent on Chk1 activity (Dodson et al., 2004;

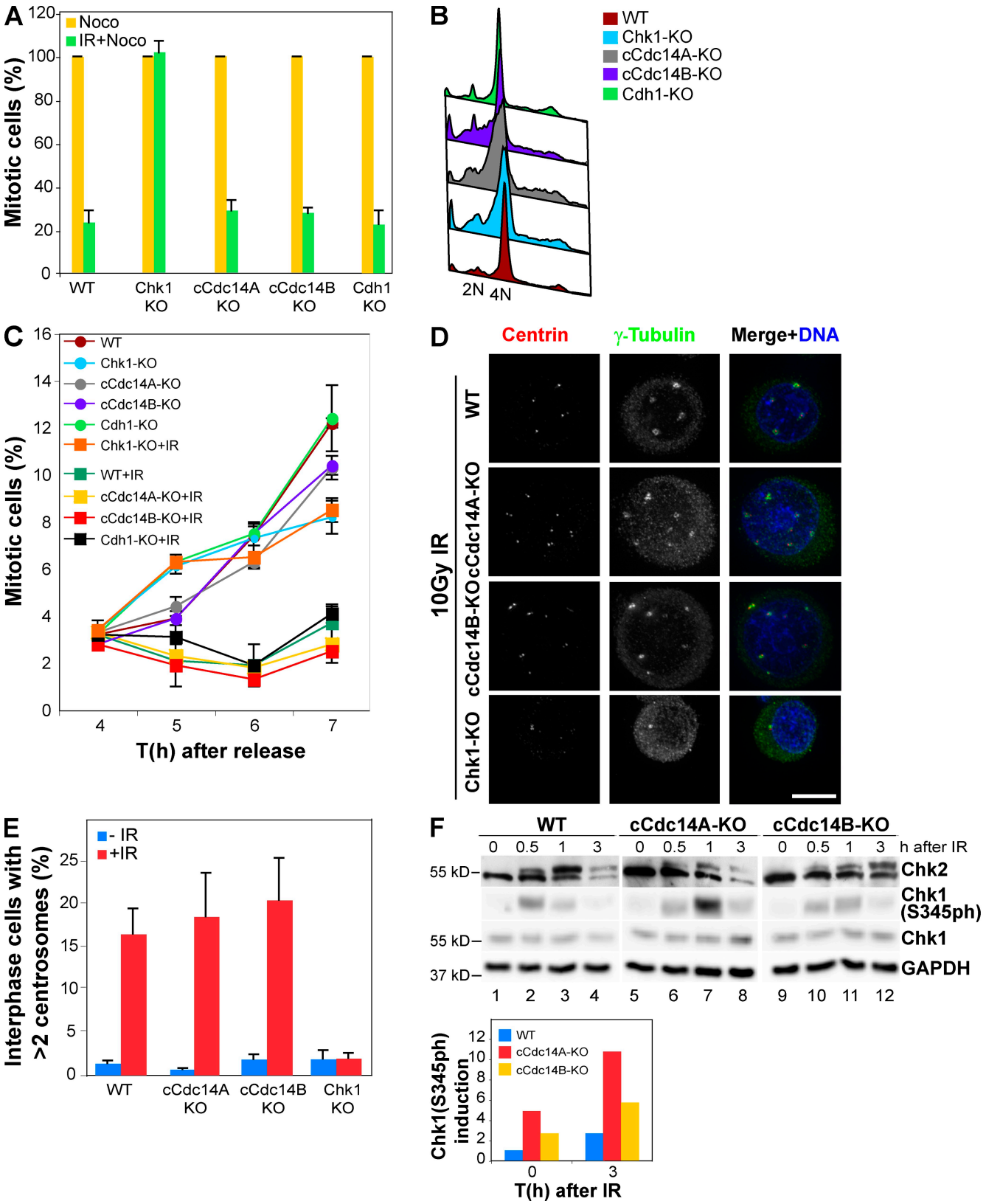

Figure 1. **Functional G2 damage checkpoint in DT40 cells deleted for cCdc14A, cCdc14B, or Cdh1.** (A) Flow cytometry analysis of the indicated cell lines incubated with Noco for 8 h with or without prior IR (IR + Noco and Noco). Cells were stained with PI and for pH3 to measure the MI. Values normalized to the MI of the corresponding Noco-treated cultures ($n = 3$). (B) Synchrony in G2 at the time of IR. (C) Cells synchronized in G2 were exposed to IR. Cells were harvested, and MI was measured by flow cytometry ($n = 3$). (D) Cells were irradiated, fixed (12 h after treatment), and stained for γ-tubulin (green) and centrin (red). The number of cells with more than two centrosomes was scored. Bar, 5 µm. (E) Quantification of phenotype in D ($n = 3$; 100 cells per each cell line) is shown. (F, top) WT, cCdc14A-KO, and cCdc14B-KO cells were analyzed by IB. (bottom) Quantification of Chk1(S345ph) before (t = 0) and after IR. Chk1(S345ph) was normalized to Chk1. Chk1(S345ph) in the untreated WT sample was set to 1 ($n = 2$). Error bars indicate mean ± SD.

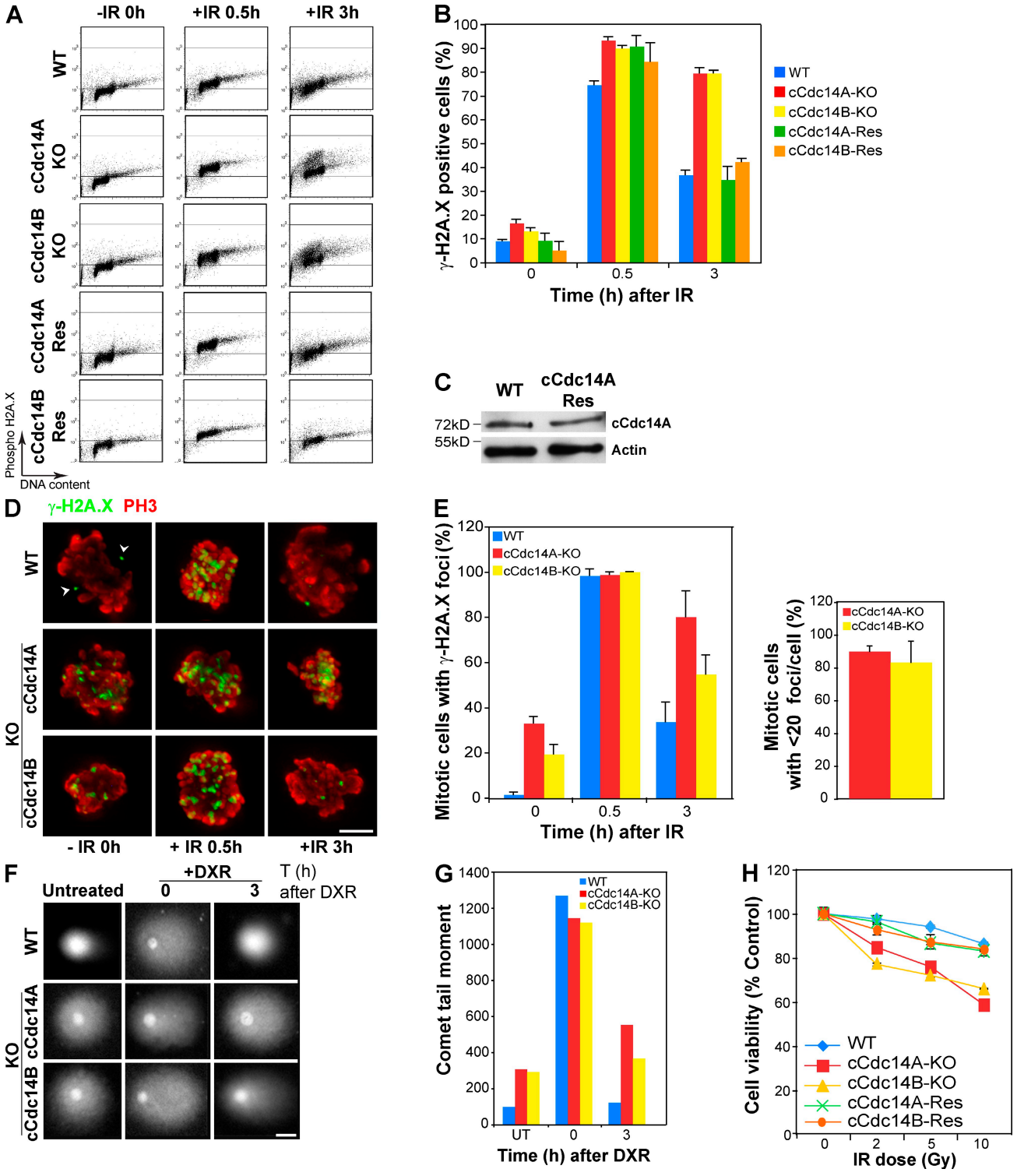

Figure 2. **Defective DNA repair in DT40 cCdc14A-KO and cCdc14B-KO cells.** (A) The indicated cell lines were harvested either before (t = 0 h) or after IR, fixed, stained with PI and anti–γ-H2A.X, and analyzed by flow cytometry. (B) Quantification of the γ-H2A.X–positive cells in A (n = 3) is shown. (C) IB analysis of cCdc14A in cCdc14A-Res cells compared with WT. (D) WT, cCdc14A-KO, and cCdc14B-KO cells harvested either before (−IR 0 h) or 0.5 and 3 h after IR. Cells were fixed, stained for pH3 (red) and γ-H2A.X (green), and examined by fluorescence microscopy. Mitotic cells before and after IR. Anti–γ-H2A.X staining of the centrosome (arrowheads) was seen in some unirradiated cells. Bar, 5 µm. (E, left) The proportion of cells positive for pH3 and γ-H2A.X was scored as a percentage of total mitotic cells (n = 3; 100 mitotic cells per genotype). (right) The number of γ-H2A.X foci/cell was counted in projected and deconvolved images of mitotic cells positive for γ-H2A.X (n = 3; 20 mitotic cells). (F) The indicated cell lines were treated ± 1.5 µM DXR for 2 h and analyzed by single-cell gel electrophoresis (comet assay). Representative images are shown. Bar, 5 µm. (G) Tail moments for each time (n = 75; mean of two independent experiments) were quantified with ImageJ software. (H) Cell viability after IR analyzed by MTT assay (n = 3; $P < 0.02$). Error bars indicate mean ± SD.

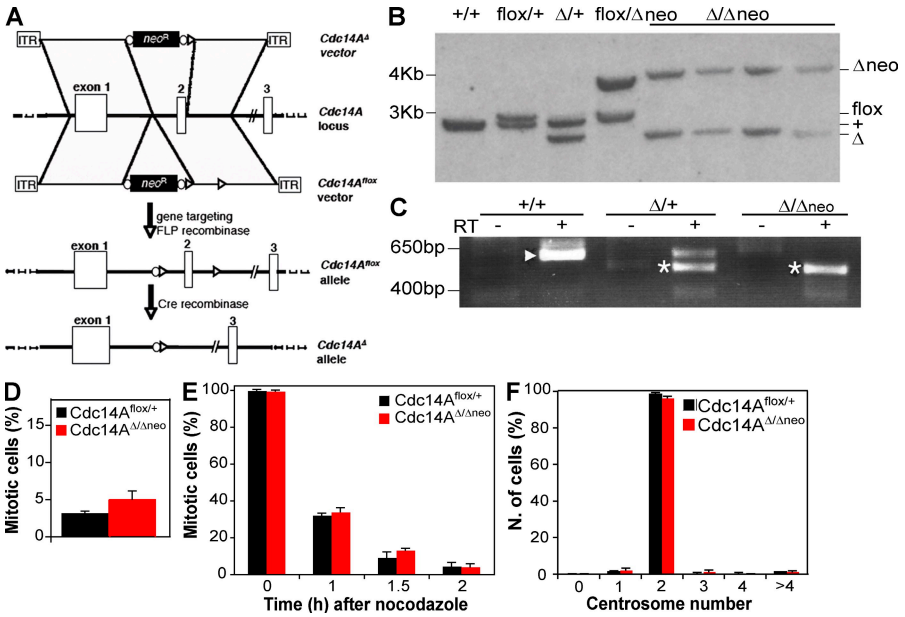

Figure 3. **Characterization of hCdc14A-deficient cells.** (A) Generation of a conditional-null hCdc14A cell line. (B) Southern blot analysis confirms biallelic mutations of the hCdc14A locus in hTERT-RPE cells. WT (+/+), flox, Δneo, and Δ alleles are marked. (C) RT-PCR analysis confirming expression of WT (arrowhead) and exon 2–deleted (asterisks) hCdc14A transcripts. (D) MI of asynchronous populations of $Cdc14A^{flox/+}$ and $Cdc14A^{\Delta/\Delta neo}$ cells. Cells were fixed and stained with Hoechst (n = 3; 300 cells per genotype). (E) $Cdc14A^{flox/+}$ and $Cdc14A^{\Delta/\Delta neo}$ cells were treated with Noco for 12 h followed by shake off into medium without Noco, fixation, and Hoechst (n = 3; 300 cells per time point). (F) Cells were fixed, stained for γ-tubulin, and categorized by centrosome number (n = 3; 200 cells per genotype). Error bars indicate mean ± SD.

Bourke et al., 2007, 2010). Cells were exposed to IR and, after 12 h, fixed and stained for γ-tubulin and centrin. As shown in Fig. 1 (D and E), WT, cCdc14A-KO, and cCdc14B-KO cells showed a 7–10-fold increase in interphase cells with more than two centrosomes after IR than in untreated cells. As expected (Bourke et al., 2010), Chk1-KO cells did not show a significant centrosome amplification after IR (Fig. 1, D and E). Collectively, these data indicate that DT40 cells lacking cCdc14A or cCdc14B have a fully functional G2 DNA damage checkpoint.

Key effectors of the G2 checkpoint are activated in response to damage in cCdc14A-KO and cCdc14B-KO cells

Protein extracts from cCdc14A-KO, cCdc14B-KO, and WT DT40 cells were analyzed by immunoblotting (IB) for the presence of checkpoint-specific markers. Chk2 activation can be monitored via a slower migrating, hyperphosphorylated isoform (Zachos et al., 2003). After IR, DT40 WT, cCdc14A-KO, and cCdc14B-KO showed Chk2 activation (Fig. 1 F, top), indicating that this aspect of the checkpoint is functional.

We next tested activation of Chk1 using an antibody against phosphorylated Chk1(S345ph) (Zachos et al., 2003). In DT40 cells, phospho-Chk1 was hardly detectable before IR, followed by a peak 0.5 h after induction of DNA damage and decreased while DNA repair proceeded (Fig. 1 F, lanes 1–4). In contrast, in cCdc14A-KO and cCdc14B-KO cells, the basal level of Chk1(S345ph) was already slightly elevated before IR (Fig. 1 F, lane 5 vs. lane 1), and this persisted even 3 h after IR (Fig. 1 F, lanes 8 and 12). This suggests that spontaneous DNA damage may already be present in untreated cCdc14-KO cells and that induced DNA damage persists for longer than in WT cells.

cCdc14A-KO and cCdc14B-KO cells exhibit impaired DNA repair

To test the possibility that the higher basal level and persistence of Chk1 phosphorylation in cCdc14A-KO or cCdc14B-KO cells (Fig. 1 F) might be related to the presence of damaged DNA, we used flow cytometry to estimate the fraction of cells bearing phosphorylated histone 2A.X (γ-H2A.X), a DNA damage marker (Furuta et al., 2003), before and after IR. The proportion of γ-H2A.X–positive WT cells decreased from nearly 100% to ∼35% 3 h after IR, whereas ∼80% of cCdc14A-KO or cCdc14B-KO cells remained positive for γ-H2A.X at this time (Fig. 2, A and B). To confirm that this phenotype was caused by inactivation of cCdc14A or cCdc14B, we stably reintroduced cCdc14A or cCdc14B cDNA into the parental nullizygous cells (cCdc14A-Res and cCdc14B-Res, respectively). cCdc14A-Res cells expressed cCdc14A at close to WT levels (Fig. 2 C). Importantly, cCdc14A-Res and cCdc14B-Res cells were essentially indistinguishable from WT in the kinetics of γ-H2A.X signal disappearance (Fig. 2, A and B).

To further investigate the kinetics of IR-induced DSB repair in WT and cCdc14-KO cells, we assessed the presence of γ-H2A.X foci by immunofluorescence (IF). In accordance with the flow cytometry analysis, 3 h after IR, ∼80% of the mitotic cCdc14A-KO cells and ∼50% of the mitotic cCdc14B-KO cells still showed multiple γ-H2A.X foci. Strikingly, a significant number of mitotic cells in unirradiated cCdc14A-KO or cCdc14B-KO cultures also contained γ-H2A.X foci (Fig. 2, D and E). It is most likely that the DSBs in untreated cells arise from failure to repair damage occurring spontaneously during the cell cycle. This raises the question of how cCdc14A-KO and cCdc14B-KO cells with a functional G2 DNA damage checkpoint are able to enter mitosis with DNA lesions. In yeast, the G2 checkpoint is sensitive to a single DSB (Bennett et al., 1997), whereas higher eukaryotes have a different sensitivity threshold (Löbrich and Jeggo, 2007), which, for mammalian fibroblasts, was calculated to be ∼20 DSBs per cell (Deckbar et al., 2007). Indeed, 80% of untreated cCdc14A-KO or cCdc14B-KO mitotic cells had <20 γ-H2A.X foci/cell (Fig. 2 E), thus explaining progression of cells bearing DNA damage into mitosis.

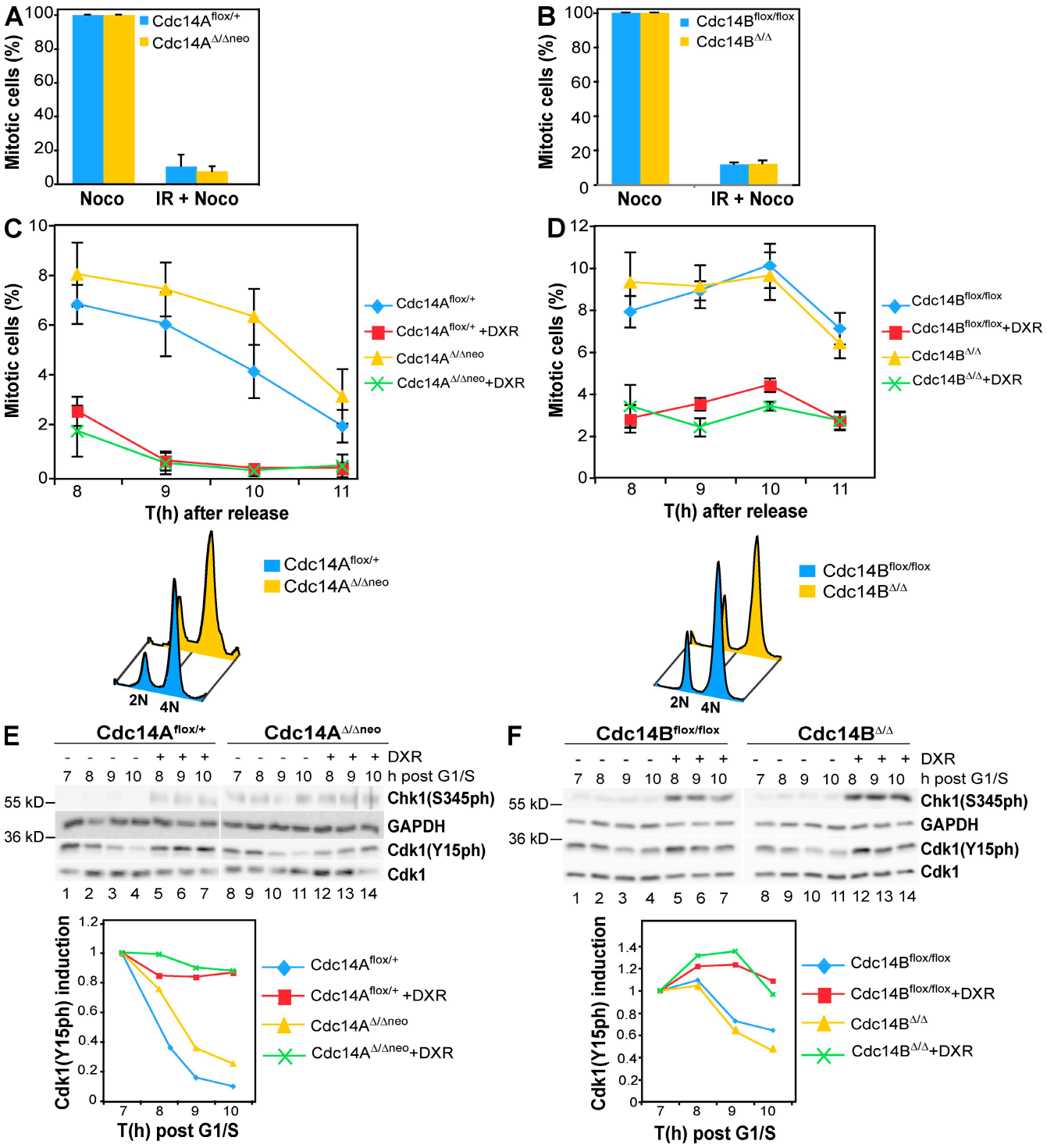

Figure 4. **Proficiency of G2 DNA damage checkpoint in hCdc14A$^{\Delta/\Delta neo}$ or hCdc14B$^{\Delta/\Delta}$ cells.** (A and B) Cells were treated for 6 (hTERT-RPE) or 4 h (HCT116) with Noco with or without prior IR. Fixed cells were stained with PI and pH3 (n = 3; MI of irradiated cells normalized to corresponding unirradiated cells). (C, top) Cdc14A$^{flox/+}$ and Cdc14A$^{\Delta/\Delta neo}$ cells were treated with thymidine for 24 h and released for 7 h to reach G2 followed by treatment with or without DXR for 1 h. At the indicated times after release, cells were fixed and stained with PI and pH3. Flow cytometry is shown (n = 3). (bottom) Synchrony in G2 at time of DXR treatment. (D, top) Cdc14B$^{flox/flox}$ and Cdc14B$^{\Delta/\Delta}$ cells were synchronized in G1/S by double-thymidine block and released for 7 h and then as in C (n = 3). (bottom) Synchrony in G2 at the time of DXR treatment. (E, top) Cdc14A$^{flox/+}$ and Cdc14A$^{\Delta/\Delta neo}$ cells were treated as in C, harvested, and analyzed by IB. (bottom) Levels of Cdk1(Y15ph) induction quantified as in Fig. 1 F. Anti-Cdk1 signals used for the normalization. (F, top) Cdc14B$^{flox/flox}$ and Cdc14B$^{\Delta/\Delta}$ cells as in D. (bottom) Levels of Cdk1(Y15ph) as in E. Error bars indicate mean ± SD.

To measure DNA damage directly, we used the comet assay (Fairbairn et al., 1995) in which DSBs confer increased electrophoretic mobility to DNA released from single cells. Consistent with the γ-H2A.X data (Fig. 2, A–E), untreated cCdc14A-KO and cCdc14B-KO cells exhibited longer comet tails compared with WT (Fig. 2 F). Treatment with DXR

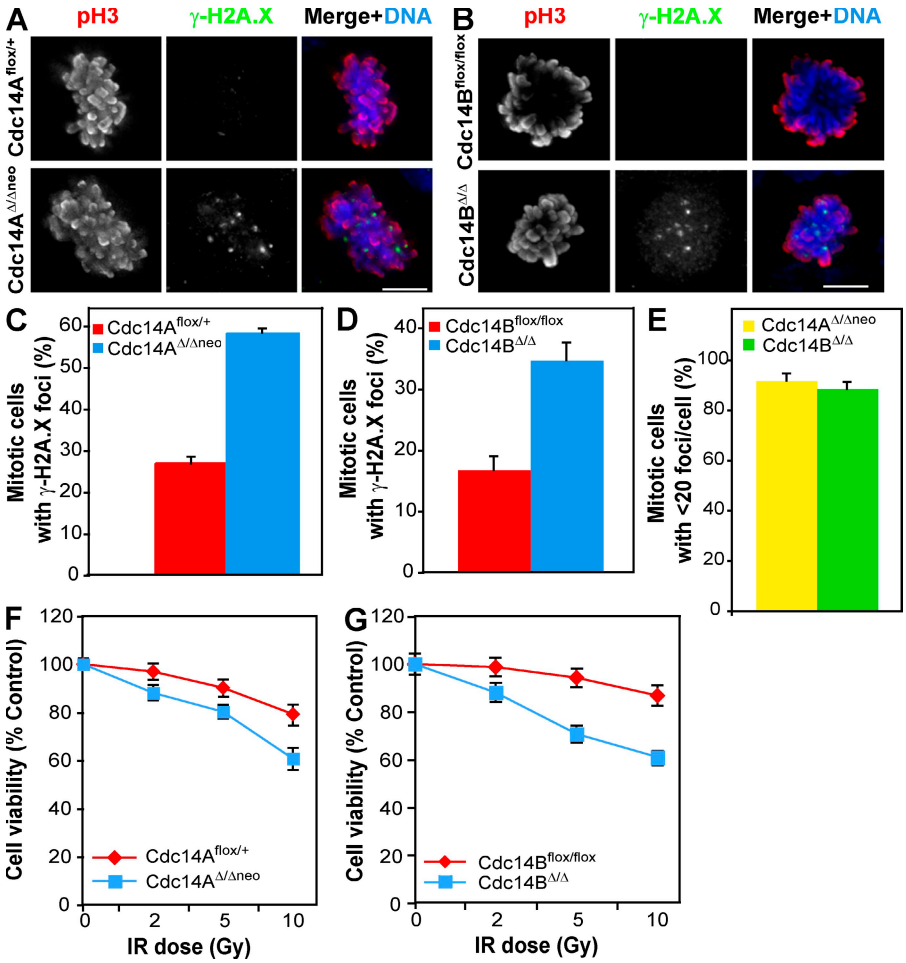

Figure 5. **Defective DNA repair in hCdc14A$^{\Delta/\Delta neo}$ or hCdc14B$^{\Delta/\Delta}$ cells.** (A and B) The indicated cell lines were fixed and stained for pH3 (red) and γ-H2A.X (green) and examined by microscopy. Mitotic cells are shown. Bars, 10 µm. (C and D) Quantification of the γ-H2A.X staining in A and B (n = 3; 100 mitotic cells per genotype). (E) Quantification of γ-H2A.X foci in mitotic cells (n = 3; 20 mitotic cells per genotype) as in Fig. 2 E. (F and G) Cell viability analyzed by MTT assay 48 h after treatment with IR (n = 3). Cells lacking hCdc14A or hCdc14B are significantly more sensitive than control cells ($P < 0.02$ and $P < 0.01$, respectively). Error bars indicate mean ± SD.

increased tails in all cell types (Fig. 2 F, t = 0). Strikingly, 3 h after treatment, DNA repair was essentially complete in WT cells, as indicated by the reduction in comet tails to control levels, whereas comet tails in cCdc14A-KO and cCdc14B-KO cells remained elevated. Based on the comet tail moment value, which quantitatively represents the extent of DNA damage (Helma and Uhl, 2000), we estimate four- to fivefold higher damage in cCdc14A-deficient cells than in control cells 3 h after DXR treatment (Fig. 2 G). Thus, cCdc14A-KO and cCdc14B-KO cells repair DSBs slower than WT cells. Consistent with the aforementioned observations, cells lacking cCdc14A or cCdc14B had reduced survival rates after IR compared with WT, cCdc14A-Res, and cCdc14B-Res cells (Fig. 2 H).

Homozygous deletion of the Cdc14A locus in human cells

To investigate the evolutionary conservation of the role of hCdc14A in the DNA damage responses, we generated a Cdc14A$^{\Delta/\Delta neo}$ cell line by disrupting both copies of Cdc14A in human telomerase reverse transcription (hTERT)–immortalized retinal pigment epithelial (RPE) cells (hTERT-RPE; Fig. 3, A–C). Cdc14A$^{\Delta/\Delta neo}$ cultures did not show any significant alteration in their MI (Fig. 3 D), in their ability to exit from mitosis (Fig. 3 E), or in centrosome number (Fig. 3 F). These findings demonstrate that hCdc14A is dispensable for viability and proliferation of an untransformed human cell line.

Human cells deficient for hCdc14A or hCdc14B have a functional G2 DNA damage checkpoint

We used Cdc14A$^{\Delta/\Delta neo}$ cells together with an hCdc14B$^{\Delta/\Delta}$ HCT116 cell line (Berdougo et al., 2008) to investigate whether hCdc14A and hCdc14B are required for G2 DNA damage checkpoint proficiency. Asynchronously growing Cdc14A$^{flox/+}$ and Cdc14A$^{\Delta/\Delta neo}$ cells were treated with Noco for 6 h with or without prior IR. Quantification of MI revealed that Cdc14A$^{\Delta/\Delta neo}$ cells arrested in G2 as efficiently as controls (Fig. 4 A). Efficient arrest also occurred after DXR treatment (unpublished data). Cdc14B$^{\Delta/\Delta}$ cells were similarly DNA damage checkpoint proficient (Fig. 4 B). Nearly identical results were obtained when cells were exposed to DNA damage after synchronization in G2 (Fig. 4, C and D).

We also monitored several markers of the DNA damage checkpoint in human cells by IB. Cdc14A$^{\Delta/\Delta neo}$ and Cdc14B$^{\Delta/\Delta}$ cells synchronized in G2 activate the main effectors of the DNA damage checkpoint, as indicated by the increased phosphorylation of Chk1 on Ser345 after treatment with DXR (Fig. 4, E and F, lanes 12–14 vs. lanes 8–11). Moreover, inhibitory phosphorylation of Cdk1 on Tyr15 decreased in untreated Cdc14A$^{\Delta/\Delta neo}$ and

$Cdc14B^{\Delta/\Delta}$ cells after release from synchronization in G2, whereas it persisted at high levels after damage (Fig. 4, E and F, lanes 9–11 vs. lanes 12–14), indicating an arrest in G2. Interestingly, as in cCdc14A-KO DT40 cells, the basal level of Chk1 phosphorylation was already elevated in unirradiated $Cdc14A^{\Delta/\Delta neo}$ cells compared with $Cdc14A^{flox/+}$ cells (Fig. 4 E, lanes 1–4 vs. lanes 8–11).

These findings prompted us to investigate whether $Cdc14A^{\Delta/\Delta neo}$ or $Cdc14B^{\Delta/\Delta}$ cells also showed an increased number of mitotic cells bearing DNA damage foci in the absence of DSB-inducing treatments (Fig. 5, A and B). The percentage of mitotic cells exhibiting γ-H2A.X foci was significantly higher in $Cdc14A^{\Delta/\Delta neo}$ and $Cdc14B^{\Delta/\Delta}$ cultures compared with controls (Fig. 5, C and D). Also, in human cells, the number of foci was usually <20 per cell (Fig. 5 E), explaining progression of these cells into mitosis. These results suggest that in human cells, Cdc14A and Cdc14B are also likely to be required for efficient DNA repair. The persistence of DNA damage foci in $Cdc14A^{\Delta/\Delta neo}$ and $Cdc14B^{\Delta/\Delta}$ cells was associated with lower survival rates than controls after IR (Fig. 5, F and G), indicating a higher sensitivity of these mutants to DNA damage.

Conclusions

In this study, we evaluate the functions of avian and human Cdc14A and Cdc14B in cells lacking these gene products. Surprisingly, Cdc14A-KO and Cdc14B-KO cells are viable and do not show severe cellular defects. With respect to Cdc14B, our findings contrast with the G2 checkpoint defect previously reported in human cells depleted for Cdc14B using siRNA (Bassermann et al., 2008). This is unlikely to be caused by cell type specificity because both avian lymphocytes and human epithelial cells genetically deleted for Cdc14B retained normal G2 checkpoint proficiency. It seems more likely that the effects of complete and permanent loss of Cdc14B function somehow differ from the more short-term and typically less-complete ablation achieved through siRNA depletion.

Although Cdc14A-KO or Cdc14B-KO cells are DNA damage checkpoint proficient, their capacity to repair DNA is diminished, resulting in the presence of a higher number of γ-H2A.X foci compared with controls. This is true even without any treatment with DNA damage–inducing agents and results in an increased sensitivity of the Cdc14-KOs to IR. Thus, these data uncover a new requirement for avian and human Cdc14A and Cdc14B in DNA repair.

Materials and methods

Generation of cCdc14A-KO and cCdc14B-KO cells

cCdc14A and cCdc14B cDNAs were isolated by RT-PCR using total RNA extracted from DT40 WT cells as template. For cCdc14A, two separate targeting vectors containing a 2.3-kb left and 3-kb right arm of homology were synthesized and cloned into Bluescript (Agilent Technologies) flanking either puromycin or blasticidin selection cassettes (Sonoda et al., 1998). After one round of targeting with the puromycin-targeting vector, drug-resistant clones were genotyped by PCR to identify $cCdc14A^{+/-}$ cells. After excision of the puromycin cassette by induction of Cre recombinase, one hemizygous clone was electroporated with a rescue vector containing the HA-tagged cCdc14A cDNA under control of the chicken β-actin promoter and a puromycin-resistant cassette (plasmid derived from pBluescript; provided by J.M. Buerstedde, Institute for Molecular Radiobiology, Munich, Germany) and selected in 0.5 µg/ml puromycin (InvivoGen). Clones expressing cCdc14A at close to endogenous levels were electroporated with the targeting vector as described previously (Saribasak and Arakawa, 2006) and selected in 30 µg/ml blasticidin to obtain a nullizygous clone. To generate the cCdc14A rescue cell line, cCdc14A-KO cells were transfected with the cCdc14A vector and selected in 0.5 µg/ml puromycin. Drug-resistant clones were screened for cCdc14A expression by IB, and a cell line with nearly endogenous levels of cCdc14A was identified and designated cCdc14A-Res.

For cCdc14B, a targeting vector containing a 3.3-kb left and 4.8-kb right arm of homology was synthesized by long-range PCR and cloned into Bluescript flanking a blasticidin selection cassette (Sonoda et al., 1998). To generate cCdc14B-deficient DT40 clones, DT40-Cre-ER cells expressing cCdc14B-HA were transfected with the targeting construct, using initially PCR and subsequently Southern blotting to genotype drug-resistant clones after selection in 30 µg/ml blasticidin (InvivoGen). To generate the cCdc14B rescue cell line, cCdc14B-KO cells were transfected with a rescue vector containing the HA-tagged cCdc14B cDNA under control of the chicken β-actin promoter and a puromycin-resistant cassette and selected in 0.5 µg/ml puromycin. Drug-resistant clones were screened for cCdc14B-HA expression by IB, and the positive clones designated cCdc14B-Res.

Generation of hCdc14A-KO cells

To generate a conditional KO of the hCdc14A locus, 5′ and 3′ homology arms were amplified from a human BAC clone (RP11-976L7) and cloned into a vector containing a central FRT-neo-FRT-loxP cassette. A secondary loxP site was introduced downstream of exon 2 via QuikChange mutagenesis. The entire Cdc14A insert was subcloned into pAAV. Transfection of HEK293 cells, isolation of AAV particles, and infection of hTERT-RPE cells were performed as described previously (Berdougo et al., 2009). G418-resistant colonies were screened by PCR. The neo cassette was excised from $Cdc14A^{flox\text{-}neo/+}$ cells by transfection with pCAAGS-FLPe followed by puromycin selection and limiting dilution. Individual colonies were tested for neo excision by genomic PCR and reacquisition of G418 sensitivity. Targeting of the second allele was achieved with a Cdc14A vector lacking exon 2 (pAAV-Cdc14AΔ). $Cdc14A^{flox/\Delta neo}$ cells were converted to $Cdc14A^{\Delta/\Delta neo}$ cells by infection with a recombinant adenovirus-expressing Cre recombinase. Targeted clones were confirmed by Southern blotting. The transcript from the exon 2–deleted *hCdc14A* gene contains a frameshift and does not code for a functional hCdc14A protein.

Cell culture and treatments

DT40 B-lymphoma cells DT40 B-lymphoma cells were grown in DME (Invitrogen) containing 10% FBS, 1% chicken serum, 1% glutamine, 1% sodium pyruvate, 10^{-5} M β-mercaptoethanol, penicillin, and streptomycin at 40°C. HCT116 cells were grown in McCoy's 5A medium (Invitrogen) supplemented with 10% FBS (Invitrogen) at 37°C. hTERT-RPE1 cell lines were grown in DME/F-12 medium supplemented with 10% FBS, 1% glutamine, and 0.348% sodium bicarbonate at 37°C.

Cells were irradiated with 10 Gy IR using a caesium source (Gamma Cell 1000; Atomi Energy of Canada Ltd) and treated with 0.5 µg/ml Noco (Sigma-Aldrich), 5 µM aphidicolin (Sigma-Aldrich), 2 mM thymidine (Sigma-Aldrich), 5 mM caffeine (Sigma-Aldrich), 1.5 µM DXR (Applichem), and 0.1 mM 4-hydroxytamoxifen (Sigma-Aldrich) as appropriate.

Flow cytometry

Cells were fixed in 70% ethanol in PBS overnight. For DNA content analysis, cells were pelleted and resuspended in PBS containing 1 mg/ml RNase (Sigma-Aldrich) and 10 mg/ml propidium iodide (PI) incubated at room temperature for 30 min then analyzed using a flow cytometer (FACScan; BD).

For MI determinations, fixed cells were incubated with polyclonal anti–phospho histone H3 antibodies followed by FITC-conjugated secondary antibody (Invitrogen). Cells were counterstained with propidium iodide and analyzed for FITC fluorescence and DNA content by flow cytometry.

For determination of γ-H2A.X foci, fixed cells were incubated with monoclonal anti–γ-H2A.X antibody followed by FITC-conjugated secondary antibody and counterstained with propidium iodide.

IB

Cell extracts were prepared in RIPA buffer (150 mM NaCl, 1% NP-40, 0.5% Na deoxycholate, 0.1% SDS, 50 mM Tris-Cl, pH 8.0, 1 mM PMSF, complete protease inhibitor cocktail [Roche], and PhosStop phosphatase inhibitor cocktail [Roche]), resolved by SDS-PAGE, and blotted onto nitrocellulose membranes (GE Healthcare). Antibodies against Chk1(S345ph) (Cell Signaling Technology), Chk1 (G-4; Santa Cruz Biotechnology, Inc.), Cdk1(Y15ph) (IL-15; Santa Cruz Biotechnology, Inc.), and Cdk1 (cl 17;

Santa Cruz Biotechnology, Inc.) were used for IB. A polyclonal rabbit antiserum specific for avian cCdc14A was generated against the C-terminal 257 amino acids of the protein. The antibody against Chk2 was described previously (Zachos et al., 2003). Blots were scanned using a luminescence fluorimager (LAS4000; Fujifilm) and quantified using Multi Gauge software (Fujifilm).

IF and microscopy

Antibodies against γ-tubulin (GTU-88; Sigma-Aldrich), cCdc14A, GFP (purified in house), fibrillarin (4G9-E4; Cytoskeleton, Inc.), B23 (C-19; Santa Cruz Biotechnology, Inc.), γ-H2A.X(S139) (Millipore), and pH3(S10) (Millipore) were used for IF. In brief, cells were either grown on coverslips or allowed to attach to polylysine slides (VWR International), fixed with 4% paraformaldehyde for 10 min at 37°C, permeabilized with PBS-T (PBS + 0.1% Triton X-100), and blocked with 10% FBS in PBS-T for 30 min at 37°C before application of primary antibody. Alternatively, cells were fixed in 100% methanol at −20°C for 5 min. Alexa Fluor 488– and 594–conjugated secondary antibodies (Invitrogen) were used. For the detection of γ-H2A.X foci, cells were fixed with 3.7% formaldehyde in PBS for 15 min, permeabilized with 0.1% Triton X-100 in PBS for 10 min, and blocked with 10% fetal calf serum and 0.5% bovine serum albumin in PBS for 30 min. Anti-pH3 and –γ-H2A.X were diluted 1:100 in blocking buffer. Cells were incubated with the antibodies for 60 min and washed three times for 5 min in blocking buffer. Anti–rabbit Alexa Fluor 594 and anti–mouse Alexa Fluor 488 (Invitrogen) were each used at 1:500 dilution in blocking buffer. Cells were incubated with the secondary antibodies for 60 min, washed twice for 5 min with blocking buffer, and once for 5 min with PBS before being mounted in ProLong gold (Invitrogen).

Images were taken on a microscope (DeltaVision RT; Applied Precision) equipped with GFP and TRITC filters (Chroma Technology Corp.), a Plan Apo 100× NA 1.4 oil immersion objective (IX70; Olympus), softWoRx software (Applied Precision), and a camera (CoolSNAP HQ; Photometrics). Image stacks were deconvolved and projected using softWoRx.

Single-cell gel electrophoresis (alkaline comet) assay

Single-cell comet assays were performed as per the manufacturer's instructions (Trevigen). Nuclei were visualized using epifluorescent illumination on a microscope (Carl Zeiss, Inc.), and images were analyzed using ImageJ software (National Institutes of Health).

Cell viability assay

Treated or untreated cells were seeded in octuplicate microtiter wells at 5×10^3 cells/well for hTERT-RPE1 and HCT116 or at 10^5 cells/well for DT40, incubated overnight, and irradiated or grown in medium for 48 h or 24 h, respectively. Viability was measured by method of transcriptional and translational (MTT) assay. Results were expressed as the OD_{550} relative to that of untreated cells.

Online supplemental material

Fig. S1 shows localization of cCdc14A and cCdc14B, cCdc14A-KO strategy, and confirmation of KO. Fig. S2 shows cCdc14B-KO strategy, confirmation of cCdc14B-KO cells, and absence of growth defects in cCdc14B-KO cells. Fig. S3 shows localization of cCdc14A and cCdc14B after IR and absence of adaptation. Online supplemental material is available at http://www.jcb.org/cgi/content/full/jcb.200910057/DC1.

We are grateful to Dr. J.-M. Buerstedde for plasmids, the DT40 Cre-ER cell line, and advice.

This work was supported by the Deutsche Forschungsgemeinschaft (grant Schi295-3).

Submitted: 8 October 2009
Accepted: 20 April 2010

References

Bassermann, F., D. Frescas, D. Guardavaccaro, L. Busino, A. Peschiaroli, and M. Pagano. 2008. The Cdc14B-Cdh1-Plk1 axis controls the G2 DNA-damage-response checkpoint. *Cell.* 134:256–267. doi:10.1016/j.cell.2008.05.043

Bennett, C.B., J.R. Snipe, and M.A. Resnick. 1997. A persistent double-strand break destabilizes human DNA in yeast and can lead to G2 arrest and lethality. *Cancer Res.* 57:1970–1980.

Berdougo, E., M.V. Nachury, P.K. Jackson, and P.V. Jallepalli. 2008. The nucleolar phosphatase Cdc14B is dispensable for chromosome segregation and mitotic exit in human cells. *Cell Cycle.* 7:1184–1190.

Berdougo, E., M.E. Terret, and P.V. Jallepalli. 2009. Functional dissection of mitotic regulators through gene targeting in human somatic cells. *Methods Mol. Biol.* 545:21–37. doi:10.1007/978-1-60327-993-2_2

Bourke, E., H. Dodson, A. Merdes, L. Cuffe, G. Zachos, M. Walker, D. Gillespie, and C.G. Morrison. 2007. DNA damage induces Chk1-dependent centrosome amplification. *EMBO Rep.* 8:603–609. doi:10.1038/sj.embor.7400962

Bourke, E., J.A. Brown, S. Takeda, H. Hochegger, and C.G. Morrison. 2010. DNA damage induces Chk1-dependent threonine-160 phosphorylation and activation of Cdk2. *Oncogene.* 29:616–624. doi:10.1038/onc.2009.340

Buerstedde, J.M., and S. Takeda. 1991. Increased ratio of targeted to random integration after transfection of chicken B cell lines. *Cell.* 67:179–188. doi:10.1016/0092-8674(91)90581-I

Cho, H.P., Y. Liu, M. Gomez, J. Dunlap, M. Tyers, and Y. Wang. 2005. The dual-specificity phosphatase CDC14B bundles and stabilizes microtubules. *Mol. Cell. Biol.* 25:4541–4551. doi:10.1128/MCB.25.11.4541-4551.2005

Deckbar, D., J. Birraux, A. Krempler, L. Tchouandong, A. Beucher, S. Walker, T. Stiff, P. Jeggo, and M. Löbrich. 2007. Chromosome breakage after G2 checkpoint release. *J. Cell Biol.* 176:749–755. doi:10.1083/jcb.200612047

Dodson, H., E. Bourke, L.J. Jeffers, P. Vagnarelli, E. Sonoda, S. Takeda, W.C. Earnshaw, A. Merdes, and C. Morrison. 2004. Centrosome amplification induced by DNA damage occurs during a prolonged G2 phase and involves ATM. *EMBO J.* 23:3864–3873. doi:10.1038/sj.emboj.7600393

Dryden, S.C., F.A. Nahhas, J.E. Nowak, A.S. Goustin, and M.A. Tainsky. 2003. Role for human SIRT2 NAD-dependent deacetylase activity in control of mitotic exit in the cell cycle. *Mol. Cell. Biol.* 23:3173–3185. doi:10.1128/MCB.23.9.3173-3185.2003

Fairbairn, D.W., P.L. Olive, and K.L. O'Neill. 1995. The comet assay: a comprehensive review. *Mutat. Res.* 339:37–59.

Furuta, T., H. Takemura, Z.Y. Liao, G.J. Aune, C. Redon, O.A. Sedelnikova, D.R. Pilch, E.P. Rogakou, A. Celeste, H.T. Chen, et al. 2003. Phosphorylation of histone H2AX and activation of Mre11, Rad50, and Nbs1 in response to replication-dependent DNA double-strand breaks induced by mammalian DNA topoisomerase I cleavage complexes. *J. Biol. Chem.* 278:20303–20312. doi:10.1074/jbc.M300198200

Helma, C., and M. Uhl. 2000. A public domain image-analysis program for the single-cell gel-electrophoresis (comet) assay. *Mutat. Res.* 466:9–15.

Kaiser, B.K., Z.A. Zimmerman, H. Charbonneau, and P.K. Jackson. 2002. Disruption of centrosome structure, chromosome segregation, and cytokinesis by misexpression of human Cdc14A phosphatase. *Mol. Biol. Cell.* 13:2289–2300. doi:10.1091/mbc.01-11-0535

Löbrich, M., and P.A. Jeggo. 2007. The impact of a negligent G2/M checkpoint on genomic instability and cancer induction. *Nat. Rev. Cancer.* 7:861–869. doi:10.1038/nrc2248

Mailand, N., C. Lukas, B.K. Kaiser, P.K. Jackson, J. Bartek, and J. Lukas. 2002. Deregulated human Cdc14A phosphatase disrupts centrosome separation and chromosome segregation. *Nat. Cell Biol.* 4:317–322. doi:10.1038/ncb777

Queralt, E., and F. Uhlmann. 2008. Cdk-counteracting phosphatases unlock mitotic exit. *Curr. Opin. Cell Biol.* 20:661–668. doi:10.1016/j.ceb.2008.09.003

Rosso, L., A.C. Marques, M. Weier, N. Lambert, M.A. Lambot, P. Vanderhaeghen, and H. Kaessmann. 2008. Birth and rapid subcellular adaptation of a hominoid-specific CDC14 protein. *PLoS Biol.* 6:e140. doi:10.1371/journal.pbio.0060140

Saribasak, H., and H. Arakawa. 2006. Targeted transfection of DT40 cells. *Subcell. Biochem.* 40:419–421.

Sonoda, E., M.S. Sasaki, J.M. Buerstedde, O. Bezzubova, A. Shinohara, H. Ogawa, M. Takata, Y. Yamaguchi-Iwai, and S. Takeda. 1998. Rad51-deficient vertebrate cells accumulate chromosomal breaks prior to cell death. *EMBO J.* 17:598–608. doi:10.1093/emboj/17.2.598

Stegmeier, F., and A. Amon. 2004. Closing mitosis: the functions of the Cdc14 phosphatase and its regulation. *Annu. Rev. Genet.* 38:203–232. doi:10.1146/annurev.genet.38.072902.093051

Sudo, T., Y. Ota, S. Kotani, M. Nakao, Y. Takami, S. Takeda, and H. Saya. 2001. Activation of Cdh1-dependent APC is required for G1 cell cycle arrest and DNA damage-induced G2 checkpoint in vertebrate cells. *EMBO J.* 20:6499–6508. doi:10.1093/emboj/20.22.6499

Wu, J., H.P. Cho, D.B. Rhee, D.K. Johnson, J. Dunlap, Y. Liu, and Y. Wang. 2008. Cdc14B depletion leads to centriole amplification, and its overexpression prevents unscheduled centriole duplication. *J. Cell Biol.* 181:475–483. doi:10.1083/jcb.200710127

Xu, B., S.T. Kim, D.S. Lim, and M.B. Kastan. 2002. Two molecularly distinct G(2)/M checkpoints are induced by ionizing irradiation. *Mol. Cell. Biol.* 22:1049–1059. doi:10.1128/MCB.22.4.1049-1059.2002

Zachos, G., M.D. Rainey, and D.A. Gillespie. 2003. Chk1-deficient tumour cells are viable but exhibit multiple checkpoint and survival defects. *EMBO J.* 22:713–723. doi:10.1093/emboj/cdg060